When this is substituted in (II23) we finally obtain the desired expression

$$S(\mu_1,\mu_2)=[\mu_1'+\mu_2']^{-1}\mathfrak{J}(\mu_1)\mathfrak{J}(\mu_2)\times\{[Z(\mu_1')]^{-1}+[Z(\mu_2')]^{-1}\} \quad \text{(II26)}$$

as stated in the text.

APPENDIX III

To carry out the expansion leading to Eq. (124) we consider integral representations for the functions $P(\Delta\omega)$, $\mathfrak{L}(a+\Delta\omega)$, and $\exp\{-(a+\Delta\omega)^2/(Ku)^2\}$:

$$P(\Delta\omega)=(2\pi)^{-1}\int_0^\infty dt\,\exp\{-i\Delta\omega t-\Gamma(1-i)t^{1/2}\}+\text{c.c.},$$

$$\mathfrak{L}(a+\Delta\omega)=\tfrac{1}{2}\gamma\int_{-\infty}^{\infty}dt\,\exp\{-\gamma\,|\,t\,|+i(a+\Delta\omega)t\},\quad \text{with}\quad \gamma>0$$

$$\exp\{-(a+\Delta\omega)^2/(Ku)^2\}=\tfrac{1}{2}\pi^{-1/2}Ku\int_{-\infty}^{\infty}dt\times\exp\{+i(a+\Delta\omega)t-\tfrac{1}{4}(Ku)^2t^2\}.$$

By substituting the above expressions into Eqs. (123) and (124) we obtain

$$i_1(a,Ku)\equiv\int_{-\infty}^{\infty}d\Delta\omega\,P(\Delta\omega)\exp\{-(a+\Delta\omega)^2/(Ku)^2\}$$

$$=\tfrac{1}{2}\pi^{-1/2}Ku\int_0^\infty dt\exp\{-(1-i)\Gamma t^{1/2}+iat-\tfrac{1}{4}(Ku)^2t^2\}+\text{c.c.},$$

$$i_2(a,\gamma)\equiv\int_{-\infty}^{\infty}d\Delta\omega\,P(\Delta\omega)\mathfrak{L}(\Delta\omega)=\tfrac{1}{2}\gamma\int_0^\infty dt\times\exp\{-\gamma\,|\,t\,|+iat-(1-i)\Gamma t^{1/2}\}+\text{c.c.}$$

We now expand $i_2(a,\gamma)$ to first order in $\Gamma\gamma^{-1/2}$ and obtain

$$i_2(a,\gamma)=\gamma^2(\gamma^2+a^2)^{-1}-\tfrac{1}{2}\pi^{1/2}(\Gamma^2/\gamma)^{1/2}\times\mathrm{Re}[(1-i)\{\gamma(\gamma-ia)^{-1}\}^{3/2}]. \quad (123')$$

A similar expansion of $i_1(a,Ku)$ under the assumption $(|\,a\,|/Ku)\ll1$ gives

$$i_1(a,Ku)=\exp\{-a^2/(Ku)^2\}-(1.23)(2)^{1/2}(\pi)^{-1/2}(\Gamma^2/Ku)^{1/2}[1+1.479(a/Ku)]. \quad (122')$$

PHYSICAL REVIEW VOLUME 169, NUMBER 2 10 MAY 1968

Paramagnetic Resonance of Fe-Cu, Fe-Ag, and Fe-Li Associates in II–VI Compounds*

W. C. Holton, M. de Wit, and T. L. Estle†
Texas Instruments Incorporated, Dallas, Texas
and
B. Dischler
Institut für Elektrowerkstoffe, Freiburg-Br., Germany
and
J. Schneider
Physikalisches Institut der Universität, Freiburg-Br., Germany
(Received 13 December 1967)

The paramagnetic resonance of the ^6S state of Fe^{3+} has been studied in the monoclinic C_s symmetry which arises from Fe^{3+} associated with a monovalent metal impurity (Cu^+, Ag^+, or Li^+) in ZnS, ZnSe, ZnTe, CdTe, and ZnO. The Fe^{3+} and {Cu, Ag, or Li}$^+$ impurities are substitutional for the metal ions at one of the nearest possible sites. The zero-field splitting due to the crystalline electric fields is frequently large compared to the Zeeman interaction. It is observed that no specific ratio of the two quadratic fine-structure terms in the spin Hamiltonian occurs. This suggests that in many cases the observation of nearly isotropic lines near $g=4.3$ results from a fortuitous set of values for these fine-structure terms, supporting the view that a pure "rhombic" term need not follow from the symmetry of the environment.

I. INTRODUCTION

THE role of copper in the luminescent behavior of the zinc and cadmium chalcogenides has been the subject of considerable investigation for several decades.[1] Recently, the technique of electron paramagnetic resonance (EPR) has been applied to the study of these materials.[1] Although some measure of understanding has been achieved for a variety of impurity centers,

* Research sponsored in part by the Air Force Office of Scientific Research, Contract No. F44620-67-C-0073.
† Present address: Physics Department, Rice University, Houston, Tex.

[1] For an excellent review see *Physics and Chemistry of II–IV Compounds*, edited by A. Aven and J. S. Prener (John Wiley & Sons, Inc., New York, 1967). See Chap. 6 by R. S. Title for spin resonance and Chap. 9 by D. Curie and J. S. Prener for luminescence.

both those which are photosensitive and those which are not, the manner in which copper is incorporated and the associated luminescence are poorly understood.[2] However, in the case when iron and copper are simultaneously present as impurities, very characteristic anisotropic EPR spectra occur which are not photosensitive. These spectra have been identified as arising from the association of iron and copper.[3] Subsequently, associates of iron and silver and of iron and lithium have also been studied.

The Fe–Cu associate has been observed in ZnS, ZnSe, ZnTe, and CdTe, the Fe–Li associate in ZnS and ZnO, and the Fe–Ag associate in ZnS. In all of these cases the EPR spectra are characterized by the absence of a nearly isotropic spectrum about an observed g factor of 2, by a moderate iron hyperfine interaction, and by the presence of a weak copper hyperfine interaction in the case of a copper associate. These features will be shown to arise for an Fe($3d^5$) ion exhibiting a zero magnetic field splitting large compared to the Zeeman energy and with a Cu($3d^{10}$), Ag($4d^{10}$), or Li($1s^2$) ion as a nearby impurity. The proposed model is that Fe($3d^5$) and the associated impurity ion are substitutional for cations at nearest possible sites. With this model there is local charge compensation, with both impurity ions in energetically favorable electron configurations. The magnitudes of the hyperfine interactions are compatible with the paramagnetism localized principally on the Fe($3d^5$). Electric fields of monoclinic symmetry occur at the Fe site due to the charged associate and a crystalline distortion near the iron site. Other possible configurations of iron and the associated impurity have also been considered but are shown to be inconsistent with the observations.

The paramagnetic resonance of Fe($3d^5$) in strong noncubic crystalline electric fields has previously been observed for iron impurities in glass,[4] kyanite,[5] andalusite,[6] topaz,[7] amethyst,[8] rutile,[9] potassium tantalate,[10] tungstates,[11–13] titanates,[14,15] ferrichrome A,[16] hemoglobin,[17] and ribonucleic acid (RNA) and deoxyribonucleic acid (DNA).[18] A discussion of the origin of the observed g factors which depend on the magnitude and symmetry of the crystal electric field is given by Castner *et al.*[4] and by Griffith.[19] A discussion of the symmetry properties of the spin Hamiltonian is given by Wickman *et al.*[16] by Troup and Hutton,[5] and by Holuj.[20] The effect of crystalline electric fields which cause the spin to align itself along preferred crystalline directions in the absence of a static magnetic field may be described by the last two terms in the spin Hamiltonian

$$\mathcal{H}=g_0\beta\mathbf{H}\cdot\mathbf{S}+D[S_z^2-\tfrac{1}{3}S(S+1)]+E(S_x^2-S_y^2), \quad (1)$$

where x, y, and z are axes related to the local crystalline fields. Fourth-order terms in the spin operators are also possible in the spin Hamiltonian and their effect will be considered later. The orbital angular momentum of the Fe($3d^5$) free ion is zero and the ground state is sixfold degenerate, $S=\frac{5}{2}$. Here g_0 has nearly the free spin value of two and is, therefore, assumed to be a scalar. If the crystalline field terms are small (i.e., D and $E\ll g_0\beta H$), the energy levels will be only slightly perturbed by the crystal field. The $M=\frac{1}{2}$ to $-\frac{1}{2}$ transition is not shifted by a perturbation in first order and a spectrum near $g=2$ will occur. The absence of a resonance near $g=2$ proves that the low-symmetry crystalline electric field terms are not weak compared to $g_0\beta H$. If the crystalline electric field is large (D or $E\geq g_0\beta H$), so that the spins prefer some crystalline direction to the magnetic field direction through a coupling to the electric field, the spins will no longer precess freely about the magnetic field direction, and the apparent g factor will be different from 2. Two special cases are easily treated: $E=0$, $D\gg g_0\beta H$; and $D=0$, $E\gg g_0\beta H$. In the first case, with $H=0$, the six degenerate spin states of the free ion are split into three Kramers doublets, with energies $W=DM^2$, $M=\pm\frac{5}{2}$, $\pm\frac{3}{2}$, $\pm\frac{1}{2}$. The $M=\pm\frac{1}{2}$ state is lowest for $D>0$. With the application of a small magnetic field, each pair splits, but $\Delta M=\pm1$ transitions are only allowed between the $M=\pm\frac{1}{2}$ states. The observed g factor parallel to the

[2] T. L. Estle, W. C. Holton, M. de Wit, R. K. Watts, A. R. Reinberg, and J. Schneider, in Proceedings of the 1966 Budapest Conference on Luminescence (to be published); M. de Wit and A. R. Reinberg, Phys. Rev. **163**, 261 (1967); J. Dieleman, S. H. de Bruin, C. Z. Van Doorn, and J. H. Haanstra, Philips Res. Rept. **19**, 311 (1964); K. Morigaki, J. Phys. Soc. Japan **19**, 1240 (1964); W. C. Holton, T. L. Estle, M. de Wit, and J. Schneider, Bull. Am. Phys. Soc. **9**, 249 (1964); R. E. Dietz, H. Kamimura, M. D. Sturge, and A. Yariv, Phys. Rev. **132**, 1559 (1963).

[3] W. C. Holton, M. de Wit, T. L. Estle, J. Schneider, and B. Dischler, Bull. Am. Phys. Soc. **11**, 330 (1965).

[4] T. Castner, Jr., G. S. Newell, W. C. Holton, and C. P. Slichter, J. Chem. Phys. **32**, 668 (1960).

[5] G. J. Troup and D. R. Hutton, Brit. J. Appl. Phys. **15**, 1493 (1964).

[6] F. Holuj, J. R. Thyer, and N. E. Hedgecock, Can. J. Phys. **44**, 509 (1966).

[7] A. B. Denison, T. C. Ensign, and L. J. Sims, Phys. Letters **24A**, 405 (1967); T. C. Ensign and A. B. Denison, Phys. Letters **25A**, 423 (1967).

[8] T. I. Barry, P. McNamara, and W. J. Moore, J. Chem. Phys. **42**, 2599 (1965).

[9] D. L. Carter and A. Okaya, Phys. Rev. **118**, 1485 (1960).

[10] W. Wemple, Ph.D. thesis, M.I.T., 1963 (unpublished). See also W. Low and E. L. Offenbacher, in *Solid State Physics*, edited by F. Seitz and D. Turnbull (Academic Press Inc., New York, 1965), Vol. 17, p. 177.

[11] M. Peter, Phys. Rev. **113**, 801 (1959).

[12] W. G. Nilsen and S. K. Kurtz, Phys. Rev. **136**, A262 (1964).

[13] R. W. Kedzie, D. H. Lyons, and M. Kestigian, Phys. Rev. **138**, A918 (1965).

[14] S. Aisenberg, H. Statz, and G. F. Koster, Phys. Rev. **116**, 811 (1959).

[15] D. J. A. Gainon, Phys. Rev. **134**, A1300 (1964); E. S. Kirkpatrick, K. A. Müller, and R. S. Rubins, Phys. Rev. **135**, A86 (1964); D. J. A. Gainon, J. Appl. Phys. **36**, 2325 (1965).

[16] H. H. Wickman, M. P. Klein, and D. A. Shirley, J. Chem. Phys. **42**, 2113 (1965).

[17] J. E. Bennett, J. F. Gibson, and D. J. E. Ingram, Proc. Roy. Soc. (London) **A240**, 67 (1957); J. S. Griffith, Proc. Roy. Soc. (London) **A235**, 23 (1956).

[18] W. M. Walsh, L. W. Rupp, and B. J. Wyluda, in *Proceedings of the First International Conference on Paramagnetic Resonance, Jerusalem, 1962*, edited by W. Low (Academic Press Inc., New York, 1963), Vol. 2, p. 836.

[19] J. S. Griffith, Mol. Phys. **8**, 213 (1964); **8**, 217 (1964).

[20] F. Holuj, Can. J. Phys. **44**, 503 (1966).

z axis is $g_{\parallel}=2$ and perpendicular to the z axis is $g_{\perp}=6$. For the second case there are again three Kramers doublets for $H=0$ which are split by a small H, with the observed g factors having the principal values 9.678, 0.857, and 0.607 for the upper and lower doublets and having the value $g=4.29$ for the central doublet. Fe–Cu associates in ZnS are nearly described by the second case. EPR spectra are observed for the lowest and central Kramers doublets. Fe–Cu associates in ZnTe are nearly described by the first case with $D>0$, and EPR spectra are observed only for the lowest Kramers doublet. The remaining cases are intermediate, i.e., either $g_0\beta\mathbf{H}$ is not small compared to the zero-field splitting or E is comparable to D.

The experimental procedure is described in Sec. II, and the results in terms of the observed g factors are presented in Sec. III. A more complete theoretical description in terms of the full spin Hamiltonian and the fitting of experimental data to spin-Hamiltonian parameters is given in Sec. IV. Finally, Sec. IV also discusses the proposed model in the light of the obtained parameters. Section V discusses the results.

II. EXPERIMENTAL PROCEDURE

The EPR measurements were made at 9, 24, and 35 GHz. The 9-GHz spectrometer is a superheterodyne one which generates reference power for a balanced crystal receiver in a single-sideband modulator. In this way the klystron can be phase-locked to the sample cavity. The noise figure is 7.5 dB with 1N23G receiver crystals. Vertical right-circular-cylindrical TE_{011} mode cavities of several different modifications were used. The normally degenerate TM_{111} mode is shifted in frequency from the TE_{011} mode by an annular groove cut in the end wall adjacent to the cylindrical surface. This results in a loaded Q of $\sim 10^4$ for the TE_{011} mode. In one cavity the sample is mounted with a cleaved face against a small platform which rotates about a horizontal axis passing radially through the center of the cavity. The two degrees of freedom which result, the second arising because the magnet rotates about a vertical axis, permit precise alignment of any crystal axis not parallel to the platform rotation axis along the direction of the static magnetic field. In most cases spectra are taken with the $(1\bar{1}0)$ plane parallel to the plane of the magnet rotation to within 1.0°, since the [111], [110], and [001] directions lie in the $(1\bar{1}0)$ plane. The microwave cavity is enclosed within an appropriate Dewar system and adjustments to the platform angle and cavity match are made externally. The sample temperature is either near 77°K or may be set between 4.2 and 1.3°K, the latter achieved by immersing the cavity in liquid helium. A second cavity has been used to investigate the frequency dependence of the spectra at 9 GHz. This cavity is of extra length so that it may be operated in the TE_{011} mode at $\sim$8.9 GHz or in the TE_{013} mode at $\sim$9.6 GHz. The sample orientation and position remain fixed when changing frequency. In this way slight changes in g factor with frequency may be accurately measured.

EPR signals are detected either as derivatives of the absorption lines in the usual manner with lock-in detection and a recorder or, for rapid and unambiguous angular dependence determination, as the direct absorption on an oscilloscope using 50-G field modulation. A second oscilloscope trace provides field measurement by a proton nuclear magnetic resonance, which has been calibrated against Cr^+ impurities in ZnS. The 24-GHz spectrometer is a lower sensitivity homodyne instrument which also employs a TE_{011} mode cylindrical cavity. The 35-GHz spectrometer is a Varian instrument.

The II–VI compound crystals used in this work have been obtained from a variety of sources and the results in every instance are similar. ZnTe and CdTe form single sphalerite-structure crystals, and ZnO forms single wurtzite-structure crystals. The ZnS crystals used are microscopically twinned by having stacking faults along a particular ⟨111⟩ direction, which is the growth axis, denoted by $[111]_w$. Consequently, within a single specimen there are two cubic regions with the $[111]_w$ axis in common but with one region rotated 60° about this axis with respect to the other. Intermediate regions of hexagonal structure can occur as a consequence of stacking faults. Thus, the hexagonal c axis coincides with $[111]_w$. Impurities apparently occur randomly in both twins. ZnSe crystals used for this work contain similar stacking faults at macroscopic intervals, only a few occurring in a given crystal. As shown in Fig. 1 the coordination about any substitutional site is fourfold. The angular dependence of EPR spectra obtained by rotating the magnetic field in the $(1\bar{1}0)$ plane which contains $[111]_w$ shows mirror symmetry about $[111]_w$ or the c axis for impurities in the cubic or hexagonal regions. Except for the wurtzite ZnO crystals, the cleavage faces are {110} planes, which, in the case of the twinned crystals, contain $[111]_w$. There is evidence of small angle grain boundaries in some of the sphalerite crystals.

The samples containing the Fe–Cu associate are prepared either by first a diffusion of iron and then of copper from evaporated metallic layers on the nominally pure crystal or by a simultaneous diffusion. The diffusions are done in sealed quartz capsules at temperatures within a few hundred degrees of the melting points of the crystals for periods of 10 to 100 h. The ZnS crystals are brown to black after this treatment. For ZnS the diffusion is done in a sulfur atmosphere; for ZnSe, ZnTe, and CdTe, the diffusion is first done in an atmosphere of the metal and followed by heating of the crystal in either Se or Te atmosphere, as appropriate, to increase the resistivity of the sample. The associates may also be prepared by starting with crystals already containing Fe and by copper diffusions at much lower temperatures for longer periods of time. The associa-

TABLE I. ZnS:Fe–Cu centers: $(1\bar{1}0)$ –plane, $\nu_e = 9.15$ GHz, $T = 1.3$°K, number of centers = 24.

Maximum g factors Expt.	Calc.	Angles with respect to [111] of maximum g factors Expt.	Calc.	Minimum g factors Expt.	Calc.	Angles with respect to [111] of minimum g factors Expt.	Calc.
$g_z = 9.663 \pm 0.001$	Fit	18.0°±0.5°	18.4°	$g_x = 1.265 \pm 0.001$	Fit	71.6°±0.1°	71.6°
$g_z = 9.663 \pm 0.001$	Fit	51.5°±0.5°	52.1°	$g_x = 1.265 \pm 0.001$	Fit	37.8°±0.1°	37.9°
9.248 ± 0.01	9.258	10.0°±0.5°	9.3°	$g' = 0.725 \pm 0.001$	Fit	80.5°±0.2°	80.6°
9.248 ± 0.01	9.258	80.0°±0.5°	79.9°	$g' = 0.725 \pm 0.001$	Fit	10.2°±0.2°	10.0°
7.074 ± 0.007	7.052	33.5°±1.0°	32.2°	$g'' = 0.922 \pm 0.001$	0.903	59.6°±0.2°	57.3°
7.074 ± 0.007	7.052	76.3°±0.5°	77.3°	$g'' = 0.922 \pm 0.001$	0.903	12.5°±0.5°	13.3°

tion of the Fe and Cu is a consequence of the low temperature at which the associate forms relative to its binding energy. Preparation of the Fe–Ag associate is more difficult. A ZnS crystal containing iron was heated together with metallic silver and zinc for 50 h at 1050°C. The ZnO crystals were doped with Li by diffusion from the hydroxide and a subsequent iron diffusion. Lithium was diffused into ZnS crystals which contained iron. Typical impurities detected by EPR are Fe^{+}, Fe^{3+}, Mn^{2+}, Cr^{+}, Ni^{3+}, various paramagnetic copper centers,[2] and self-activated centers in crystals originally grown by chemical vapor transport with a halogen.[1] Additional impurities detected by emission spectrographic analysis are Mg and Si.

III. EXPERIMENTAL RESULTS

A. ZnS: Fe–Cu

At 9 GHz and 1.3°K, the EPR spectra of ZnS: Fe–Cu associates consist of 24 very anisotropic patterns extending from 400 G to beyond 11,000 G and another set of nearly isotropic patterns near 1500 G. Figure 2 shows the experimental angular dependence of the highly anisotropic spectra. These data were obtained as described in Sec. II directly from an oscilloscope presentation. However, the numerous data points have been removed from the figure for clarity. This angular dependence can be explained by a single g tensor and 24 centers with C_s symmetry which occur in one or the other of the twinned cubic parts of the crystal. Table I shows a number of selected extrema obtained by mounting the crystal on the platform as described in Sec. II. The quality of the perfection realized in determining the principal values and orientation of the g tensor is apparent. Those experimental values in Table I marked "fit" are used to calculate the remaining values of expected extrema and these are compared in Table I with the measurements. The resulting observed g tensor is given in Table II. The angle τ (see Fig. 1) measures the amount by which g_z is rotated from [111] towards [001] in the $(1\bar{1}0)$ plane.

TABLE II. ZnS: Fe–Cu parameters.

	Experimentally obtained g tensor Lower Kramers doublet ($\nu = 9.149$ GHz)	Central Kramers doublet ($\nu = 9.149$ GHz)	Central Kramers doublet ($\nu = 23.61$ GHz)
g_x	1.2625 ± 0.0006	4.349 ± 0.016	4.24 ± 0.04
g_y	<0.6	4.530 ± 0.002	4.403 ± 0.004
g_z	9.663 ± 0.001	4.055 ± 0.005	3.785 ± 0.004
g' [a]	0.7179 ± 0.0004		
g'' [a]	0.9189 ± 0.0002		
τ	$-18.4° \pm 0.2°$		
$\Delta H_{Fe^{57}}$ [b]	7.9 G		
$\Delta H_{Cu^{63}}$ [b]	3.4 G		

Derived spin-Hamiltonian parameters

Assume	g_0	D (cm^{-1})	E (cm^{-1})	Differences[c]
$F = U = V = 0$ [d]	2.022 ± 0.008	-0.70 ± 0.11	-0.26	<0.08
$F = U = V = 0$ [e]	2.022 ± 0.008	0.74 ± 0.11	-0.22 ± 0.04	<0.08
$U = V = 0$ [e, f]	2.020	0.69	-0.20	<0.012
$F = U = 0$ [e, g]	2.018	0.67	-0.20	<0.015

[a] See Table I for definition.
[b] See Fig. 4 for meaning of ΔH.
[c] Differences between calculated and experimental g tensors.
[d] Experimental (x, y, z) used in Eq. (5).
[e] The (x, y, z) labeling the experimental values is transformed to $(y, z, x) = (\eta, \zeta, \xi)$ and Eqs. (4) and (5) are used.
[f] Calculate $F = 0.034$ cm^{-1}.
[g] Calculate $V = -0.020$ cm^{-1}.

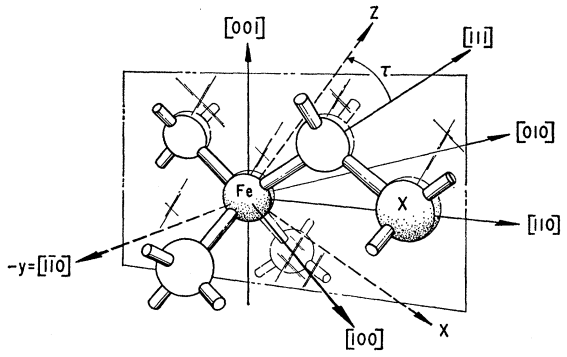

FIG. 1. Crystal-lattice model showing the Fe and Cu (or Ag, Li) impurities and the g-tensor axes.

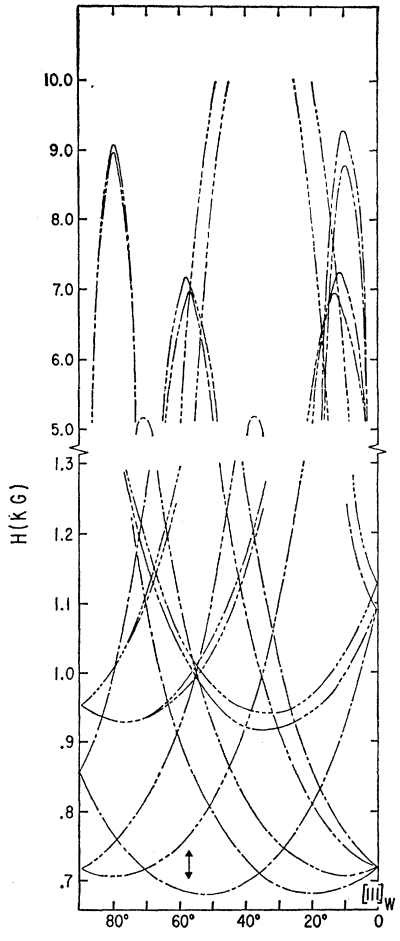

FIG. 2. Experimentally determined angular dependence of the lowest Kramers doublet EPR spectra of ZnS:Fe–Cu at 9.16 GHz, with the magnetic field in the (1$\bar{1}$0) plane. The doubling of some of the lines above 5 kG and of the lines with minima near 920 G is due to a small misalignment of the crystal. Lines originating from Fe–Cu associates, which would be magnetically equivalent if the magnetic field were exactly in the (1$\bar{1}$0) plane, are split by crystal misalignment.

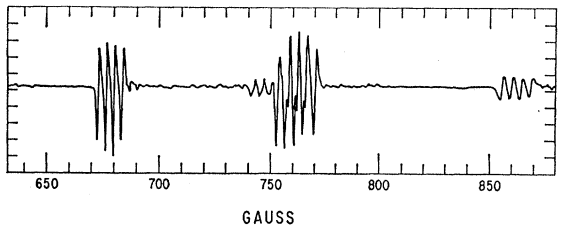

FIG. 3. The low magnetic field portion (shown by arrow in Fig. 2) of the ZnS:Fe–Cu spectrum with the magnetic field in the (1$\bar{1}$0) plane and 56.4° from $[111]_w$.

A portion of the anisotropic spectrum, at the angle indicated by the arrow in Fig. 2, is shown in Fig. 3. Each of the four-line patterns in Fig. 3 is shown in Fig. 2 as a single curve. When such a rapid angular variation is present in the spectrum the alignment of the crystal becomes critical. The effect of a small misalignment can be seen near 760 G in Fig. 3, where 2 four-line patterns are nearly superimposed and a third pattern of lower intensity is also seen. Figure 4 shows the lowest field pattern under higher resolution. The upper spectrum was obtained using a sample containing the natural isotopic abundances of Fe (2.2% Fe^{57} with $I=\frac{1}{2}$; the remainder with $I=0$). The four-line pattern is seen to arise from a hyperfine interaction with copper. The Cu^{63} and Cu^{65} isotopes appear in the correct ratios of splitting and intensity. The lower spectrum is from a sample enriched to 50% with Fe^{57}, and the additional splitting of the pattern due to the Fe^{57} hyperfine interaction is seen. The line drawing immediately below the lower spectrum shows the decomposition of the spectrum, with + and − signs for the Fe^{57} spin up or down and 0 for the spinless iron isotopes.

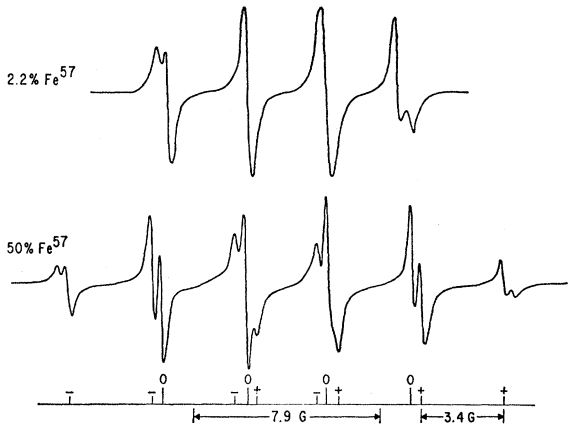

FIG. 4. High-resolution spectra of the lowest field line (see Fig. 2) of the ZnS:Fe–Cu spectra with the magnetic field in the (1$\bar{1}$0) plane and 51.5° from $[111]_w$. Frequency = 9.16 GHz and the sample temperature = 1.3°K. The upper spectrum is with the naturally occurring abundance (2.2%) of $Fe^{57}[S(Fe^{57})=\frac{1}{2}]$ and the lower spectrum is of an Fe^{57} enriched sample (50%). The decomposition of the spectra into hyperfine components is shown in the line drawing below the spectra ($A_{Fe^{57}}=7.9$ G and $A_{Cu^{63}}=3.4$ G).

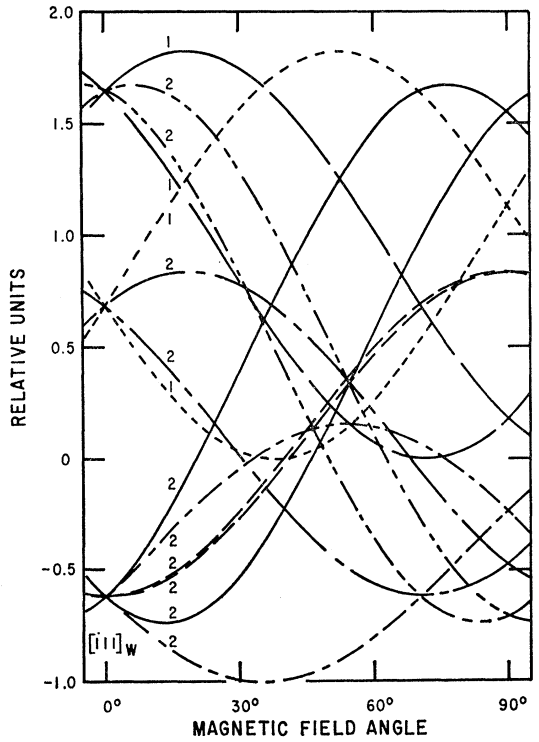

FIG. 5. The theoretical anisotropy of the central Kramers doublet for ZnS:Fe–Cu. The assumptions for the calculation are discussed in the text. Relative units are used on the ordinate and the angle between $[111]_w$ and the magnetic field in the $(1\bar{1}0)$ plane is along the abscissa. Lines which are similar by having their principal axes similarly oriented with respect to the plane of the magnetic field rotation are denoted by the same type of dashed or solid curve. The number of identical members belonging to each line is given by the number near 15°.

The copper hyperfine structure could not be followed throughout the entire angular variation of the spectrum but is only prominent and well resolved at low magnetic fields. Typical values in the low-field region are (see Fig. 4) $A_{Cu^{63}}=3.4$ G and $A_{Fe^{57}}=7.9$ G.

The calculated angular dependence of the spectrum which is observed near $g=4.3$ is shown in Fig. 5. In the experimental angular dependence the patterns, represented by a line in Fig. 5, are usually broad and overlap each other so that a complete experimental angular dependence could not be obtained. However, along some special directions such as $[111]_w$ and 90° from it, and in the relatively uncluttered regions of the angular dependence plot, the spectrum is well-enough resolved to make accurate measurements. Two principal values of the g tensor are obtained from the extreme excursions in the pattern. Altogether some 12 data points were obtained, enough to calculate the parameters and cross check them. The spectra at 9.15 GHz with the $[111]_w$ and $[1\bar{1}0]$ directions along the magnetic field are shown in Fig. 6. They can be seen at 77°K, in contrast to all but one of the other Cu centers in the chalcogenides, which have only been detected at or below 4.2°K.[2]

The copper hyperfine splitting is resolved along uncluttered directions and the Fe^{57} hyperfine splitting showed the presence of Fe in an Fe^{57}-enriched sample. The temperature dependence of the intensities of these spectra shows that they arise from a thermally populated excited state. Additional measurements have been made to investigate the frequency dependence of the g tensor, and data were obtained at 24 GHz. The observations are summarized in Table II.

The spectra near $g=4.3$ and the anisotropic ones can be explained with the same principal directions of their g tensors. Both spectra contain Fe and Cu and the spectrum near $g=4.3$ is an excited state. In addition, as will be shown in Sec. IV, the principal values of the observed g tensors arise from a common spin Hamiltonian. Both EPR spectra, therefore, arise from the same defect. The transitions are absent when the measurements are made with the microwave magnetic field parallel to the Zeeman field. Together with the low symmetry this indicates that integral spin levels are not involved in these transitions. Integral spin levels are normally expected to be admixed in the low symmetry and allowed transitions would then occur for the parallel field orientations. In addition, the EPR signals are not photosensitive. The simplest model consistent with these observations is for the Fe and Cu to be substitutional in two nearest Zn sites.

Additional weak anisotropic spectra which also display the copper hyperfine splitting are observed in the low-field (~400 G) region. The angular dependence of

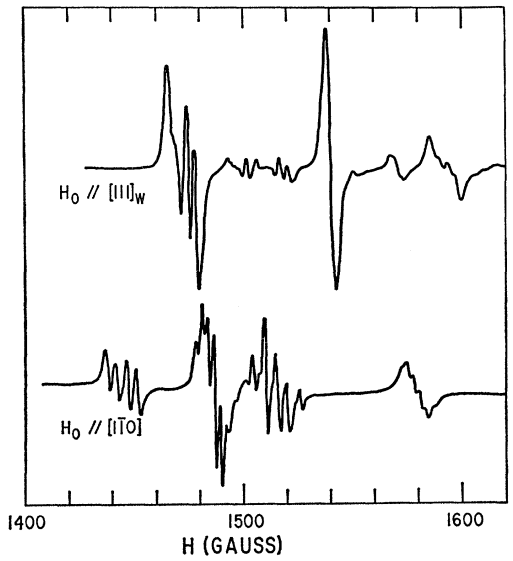

FIG. 6. EPR derivative spectra as a function of **H** (gauss) of the first excited Kramers doublet of ZnS:Fe–Cu for $[111]_w$ along **H** (upper spectrum) and for $[1\bar{1}0]$ along **H** (lower spectrum). These crystals are microscopic twins. However, for the two particular orientations chosen the two twins are equivalent with respect to **H**. The frequency is 9.093 GHz and the sample temperature is 77°K.

these spectra could not be obtained. However, one principal g factor occurring 30.5° from $[111]_w$ in the $(1\bar{1}0)$ plane is $g=8.03$. The corresponding copper hyperfine splitting is $A_{Cu^{63}}=2.5$ G. A second extremum in the pattern occurs 90° from the first in the $(1\bar{1}0)$ plane at $g=3.58$. These spectra we ascribe to Fe–Cu associates in the noncubic and presumably hexagonal regions of the ZnS crystal.

B. ZnSe: Fe–Cu

These spectra extend from 750 to 4500 G at 9 GHz. The observed angular dependence is shown in Fig. 7. The transitions corresponding to the solid curves in this figure are very weak and move rapidly when the magnetic field is rotated in the $(1\bar{1}0)$ plane. Again, each line in Fig. 7 corresponds to a four-line pattern. A sample enriched with Fe^{57} shows the additional hyperfine splitting analogous to the ZnS case. The EPR of the defect is not photosensitive. Since the crystals are macroscopic twins, there is not necessarily equal abundance of both twins present in the sample; consequently, one set of lines is observed to be weaker than the other set. The g-tensor components are given in Table III. The hyperfine-structure tensor was not determined since the lines broaden sufficiently at high fields so that the hyperfine splitting cannot be followed for an appreciable range. At the low field extreme the Cu splitting is ~5 G, with a linewidth of ~2 G.

C. ZnTe: Fe–Cu

These spectra extend from 900 to 3300 G at 9 GHz. The observed angular dependence with H in the $(1\bar{1}0)$ plane is shown in Fig. 8. The coincidence of the two crossovers at the intermediate magnetic field at 90° in Fig. 8 is accidental and, therefore, determines the angle τ accurately for this case. The splitting of some of the lines in this figure indicates a small misalignment of the crystal. Each curve represents a four-line pattern, due to the Cu hyperfine splitting. The principal values of the g tensor are given in Table III.

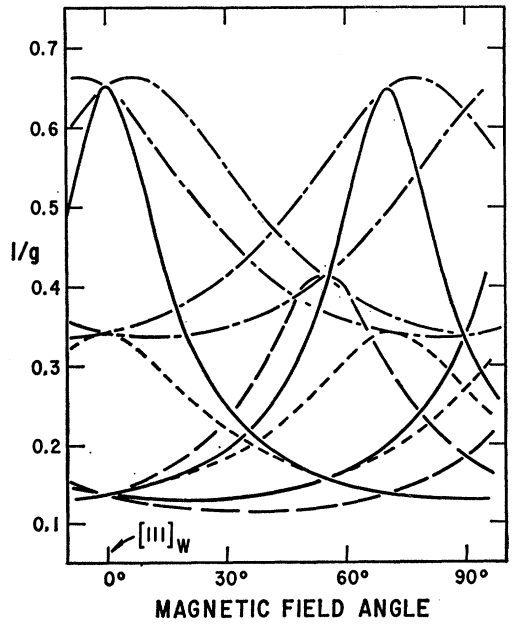

FIG. 7. Angular dependence of ZnSe: Fe–Cu spectra in the $(1\bar{1}0)$ plane.

TABLE III. Fe–Cu associate parameters for ZnSe and ZnTe. Only the lowest Kramers doublet is observed. We have assumed $D>0$.

	ZnSe	ZnTe
ν	9.16 GHz	9.13 GHz
g_x	2.987±0.002	5.301±0.002
g_y	8.794±0.004	7.292±0.004
g_z	1.515±0.002	2.015±0.002
τ	6.6°±0.2°	8.2°±0.1°
A_y (Cu)	$(21\pm1)\times10^{-4}$ cm^{-1}	...[a]
A_y (Fe^{57})	$(27\pm5)\times10^{-4}$ cm^{-1}	...[a]
E (cm^{-1})	0.1908	0.04D
D (cm^{-1})	1.377	
g_0	2.058	2.11

[a] Observed but not measured.

D. CdTe: Fe–Cu

These spectra extend from 820 to 3600 G at 9 GHz. However, they have not been analyzed because the increased linewidth, presumably due to a ligand hyperfine interaction, prevents a determination of the angular dependence. In addition, the best sample in the sense of signal-to-noise ratio contained several single-crystal regions which were separated one from another by small-angle grain boundaries.

E. ZnS: Fe–Ag

The Fe–Ag associate spectra have been studied at 9 GHz (see Fig. 9) with some additional measurements at 35 GHz. The g tensor is given in Table IV. Transitions within the lowest and central Kramers doublets occur in the same field region, but can be distinguished by their different linewidths.

F. ZnS: Fe–Li

Spectra were taken at 9 and 35 GHz. They are very similar to the ZnS: Fe–Ag case, thus indicating that the spin-Hamiltonian parameters are not much different from the Fe–Ag values. No complete analysis was undertaken.

G. ZnO: Fe–Li

The spectra of the Fe–Li associate were investigated at 35 GHz. The pure hexagonal crystal of ZnO has an

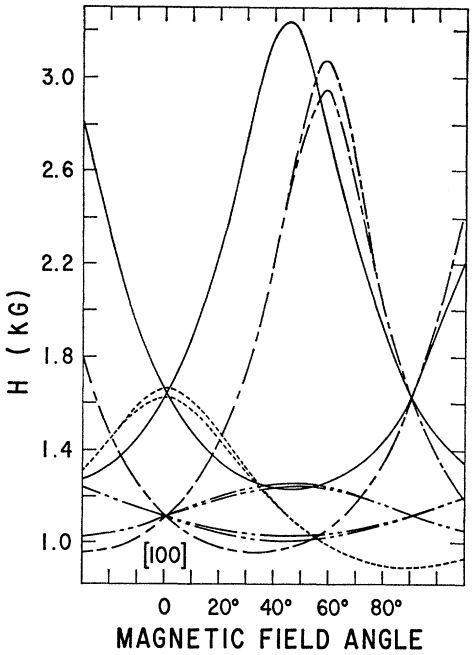

FIG. 8. Angular dependence of ZnTe:Fe-Cu spectra in the $(1\bar{1}0)$ plane as a function of the angle between [100] and the magnetic field.

axial crystalline electric field parallel to the c direction. Therefore, three types of centers are expected to occur: Fe in an axial zinc site and Li in a basal zinc site (sixfold); Li in an axial zinc site and Fe in a basal zinc site (sixfold); and both Fe and Li in basal zinc sites (twelvefold). The spectrum for $\mathbf{H} \| c$ is shown in Fig. 10. Under this orientation three fine-structure quintets are seen, one for each type of center. In addition, the resonance of nonassociated Fe^{3+} occurs, the over-all splitting of the fine-structure quintet being 5535 G. The over-all splittings of the quintets from the Fe–Li associates are 11 220, 4330, and 7200 G for $\mathbf{H} \| c$, the latter value corresponding to the twelve-fold type.

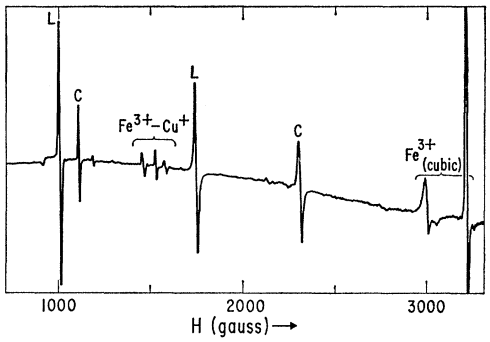

FIG. 9. Low-field portion of the spectrum of ZnS:Fe–Ag for $H \| [111]_w$ at 77°K and 9.1 GHz. The line marked Fe_{cubic} arises from nonassociated iron. For the Fe–Ag associate transitions within the lower Kramers doublet (L) and within the center doublet (C) are observed simultaneously. A weak resonance of the Fe–Cu associate is also seen.

TABLE IV. ZnS:Fe–Ag parameters.

Experimentally obtained g tensor. $\nu=9.104$ GHz.	Lower Kramers doublet	Central Kramers doublet
g_x	3.986±0.002	2.268±0.002
g_y	7.480±0.002	1.325±0.002
g_z	<1.7	5.845±0.002
τ	−4.4°±0.1°	−3.5°±0.1°

Derived-spin Hamiltonian parameters.

$g_0=2.016\pm0.001$

$D=0.325\pm0.002\ \text{cm}^{-1}$

$E=0.0248\pm0.0002\ \text{cm}^{-1}$

$F=U=V=0$

From the angular dependence it follows that the maximum zero magnetic field splitting occurs for one of the sixfold types near $\mathbf{H} \| c$ and is just twice that of the nonassociated Fe^{3+}, i.e., $D\approx0.12\ \text{cm}^{-1}$.

IV. THEORY

There are three topics we wish to consider which relate to a spin of $\frac{5}{2}$ in C_s symmetry. The first concerns the spin Hamiltonian introduced by Abragam and Pryce.[21] Instead of attempting to derive it from first principles, its form is determined entirely from symmetry considerations. With the spin Hamiltonian given, it is then of interest to consider the various possibilities

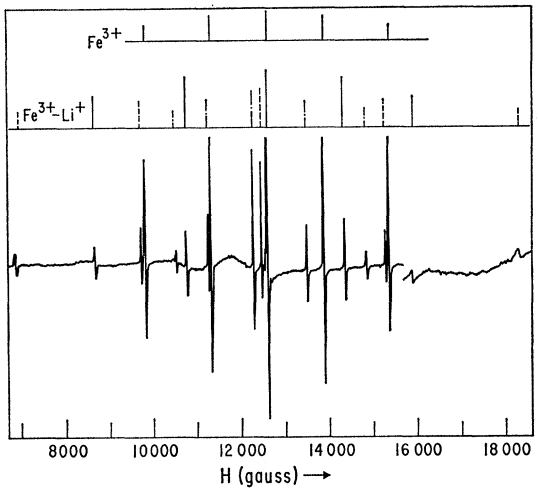

FIG. 10. Spectrum of ZnO:Fe–Li at 300°K and 35 GHz for $H \| c$. The line drawings above the spectrum show the decomposition into the several fine-structure quintets, as mentioned in the text. The strongest lines arise from nonassociated Fe^{3+}. All 15 lines expected for the Fe–Li associates under this orientation are observed. The portion at highest field is taken from a separate spectrum with lower over-all intensity.

[21] A. Abragam and M. H. L. Pryce, Proc. Roy. Soc. (London) **A205**, 135 (1951).

for the experimentally observed g factors since these range from 0.5 to 10, depending on the microwave frequency and the magnitudes of various parameters. Finally, there is the calculation of the spin-Hamiltonian parameters from first principles. It has proven difficult to determine the origin of the g shift and the crystal-field splitting even in cubic symmetry. The precise origin of the g-factor shift is still under investigation and calculations require a rather detailed knowledge of the structure of the Fe^{3+} center.[22] In addition, there is a theoretical relationship between the g-factor anisotropy and the axial field parameter in the spin Hamiltonian.[23] Such a relationship may be expected to hold also in the case of C_s symmetry, but these points are not pursued here. However, a simple theoretical treatment of the possible origin of the quadratic coefficients has been proposed by Griffith and we examine our results in the light of this theory.[19]

A. Spin Hamiltonian

Since its introduction the spin Hamiltonian $\mathcal{H}$ has been used to describe the low-lying levels which are studied by their EPR spectra. We wish to do the same here but deviate slightly from the original intent. Instead of describing each observed transition with a fictitious spin of $\frac{1}{2}$, as done in Sec. III, we prefer to describe the six lowest levels of Fe^{3+} by means of the actual spin of $\frac{5}{2}$. The reason is that the large anisotropies in the observed g factor which occur in orthorhombic symmetry are mostly a result of the mixing of the various levels by the crystalline fields and are not significant for an eventual theoretical interpretation. In addition, estimates of the crystalline field parameters can be obtained. These are more useful for comparison with theory and for comparison with Fe^{3+} in different environs since the frequency dependence of the observed g tensor is removed.

For an interpretation of the experimental data we need the form of the spin Hamiltonian for C_s symmetry. To deduce the terms from perturbation theory is quite difficult for low symmetry, and instead we use symmetry arguments only. Any indication of the magnitude of the terms is then lost, but even in a perturbation calculation these magnitudes cannot yet be obtained. The use of symmetry arguments in the determination of the spin Hamiltonian has a long history.[24] Our prescription essentially follows Griffith.[24] The number of levels to be described is $2S+1$. The crystal-field splittings are described by the irreducible tensor operators $T_m{}^l(\mathbf{S})$, of rank l, constructed from the usual spin operators S_z, S_+, and S_-, with the eigenvalues for S^2 of $S(S+1)$ and for S_z of M in units of $\hbar$. The particular form of the tensor operators may be obtained from Racah's definition.[25] The rank l of these operators in the spin Hamiltonian is even because of time reversal symmetry and $l \leq 2S$. When the symmetry is now lowered to that of the point group of the defect, the operators $T_m{}^l$ may be reduced. Only those parts which belong to the irreducible identity representation $\Gamma_1(S^l)$ of the point group considered may appear in the spin Hamiltonian. Here l is the rank of the tensor and the degree of the multinomial in the spin components S_i. In addition to these terms there are operators which describe the interaction with external fields, nuclear moments, etc. For example, the usual Zeeman term is linear in the spin operators and linear in the magnetic field. The tensor operators $T_m{}^1(\mathbf{S})$ and $T_m{}^1(\mathbf{H})$ are reduced to the irreducible representation of the point group. All possible direct products $\Gamma_i(\mathbf{S}) \times \Gamma_j(\mathbf{H})$ are taken. Of the resultant reducible representations again only the parts that reduce to Γ_1 are retained. As an example, consider $S=\frac{5}{2}$ in T_d symmetry, so that $l \leq 5$. Only the $T_m{}^4(\mathbf{S})$ reduces to a $\Gamma_1(S^4)$ representation and this is the well-known cubic crystal-field term.[21] For the Zeeman term we find that $T_m{}^1(\mathbf{H})$ transforms as Γ_4 and so does $T_m{}^1(\mathbf{S})$, and $\Gamma_4 \times \Gamma_4$ contains $\Gamma_1(SH)$ once and the coefficient of this term is the usual g factor. In addition, there are terms proportional to S^3H and S^5H. $T_m{}^3(\mathbf{S})$ reduces to $\Gamma_2+\Gamma_4+\Gamma_5$ and $T_m{}^5(\mathbf{S})$ to $\Gamma_3+2\Gamma_4+\Gamma_5$. In the direct product with $\Gamma_4(H)$ there appears one term $\Gamma_1(S^3H)$ and two terms $\Gamma_1(S^5H)$, and these three additional terms each appear with an independent coefficient in $\mathcal{H}$ and have been considered by Aisenberg *et al.*[14] Tables of the vector addition coefficients, bases for representations, full rotation group compatibility tables, etc., are available for the 32 point groups[26] and make this method particularly convenient, especially when only the number of parameters in the spin Hamiltonian is desired. Usually, the form of the various terms in the spin Hamiltonian can then be determined by inspection.

We now apply this method to the system of $S=\frac{5}{2}$ in C_s symmetry and consider only the Zeeman terms linear in the components of S. The group has two irreducible representations of dimension one, the identity representation Γ_1 with basis S_ζ and Γ_2 with basis S_ξ or S_η. The $\xi\eta$ plane is the reflection plane. Both $\mathbf{S}$ and $\mathbf{H}$ reduce to $\Gamma_1+2\Gamma_2$. The direct product contains Γ_1 five times. The Zeeman term is, therefore,

$$\beta\{g_{\xi\xi}S_\xi H_\xi+g_{\eta\eta}S_\eta H_\eta+g_{\zeta\zeta}S_\zeta H_\zeta+g_{\xi\eta}S_\xi H_\eta+g_{\eta\xi}S_\eta H_\xi\}. \tag{2}$$

[22] H. Watanabe, J. Phys. Chem. Solids **25**, 1471 (1964).

[23] H. Watanabe, in *Proceedings of the International Conference on the II-VI Semiconducting Compounds, 1967*, edited by D. G. Thomas (W. A. Benjamin, Inc., New York, 1967), p. 1381.

[24] A partial list of references is: J. M. Luttinger, Phys. Rev. **102**, 1030 (1956); G. F. Koster, *ibid.* **109**, 227 (1958); Y. Tanabe and H. Kamimura, J. Phys. Soc. Japan **13**, 394 (1958); G. F. Koster and H. Statz, Phys. Rev. **113**, 445 (1959); H. Statz and G. F. Koster, *ibid.* **115**, 1568 (1959); J. S. Griffith, Mol. Phys. **3**, 79 (1960); F. K. Kneubühl, Phys. Kondensierten Materie **1**, 410 (1963); T. Ray, Proc. Roy. Soc. (London) **A277**, 76 (1964).

[25] G. Racah, Phys. Rev. **62**, 438 (1942).

[26] G. F. Koster, J. O. Dimmock, R. G. Wheeler, and H. Statz, *Properties of the Thirty-two Point Groups* (M. I. T. Press, Cambridge, Mass., 1963).

One principal value of the g tensor is perpendicular to the symmetry plane $g_{\xi\zeta}$; two components are in the plane but arbitrarily oriented with respect to the ξ, η coordinates, determined by $g_{\xi\xi}$, $g_{\eta\eta}$, and $\frac{1}{2}(g_{\xi\eta}+g_{\eta\xi})$; and there is a skew symmetric part $\frac{1}{2}(g_{\xi\eta}-g_{\eta\xi})$. Skew symmetric terms have been considered before[27] and are difficult to detect if present.[28]

The crystal-field terms proportional to S^2 are obtained from $T_m^2(\mathbf{S})$, which reduces to $3\Gamma_1+2\Gamma_2$. The three terms in $\mathcal{H}$ are

$$E'(S_\xi^2-S_\eta^2)+D'[S_\zeta^2-\tfrac{1}{3}S(S+1)]+E''(S_\xi S_\eta+S_\eta S_\xi). \tag{3}$$

Again, the orientation of the crystal fields relative to the ξ, η coordinates is arbitrary. The terms proportional to S^4 are obtained from $T_m^4(\mathbf{S})$, which reduces to $5\Gamma_1+4\Gamma_2$, and yield

$$\begin{aligned}(F/60)[&35S_\zeta^4-30S(S+1)S_\zeta^2+25S_\zeta^2-6S(S+1)\\&+3S^2(S+1)^2]+(U_++U_-)S_+^2[7S_\zeta^2+14S_\zeta\\&-S(S+1)+9]+(U_+-U_-)S_-^2[7S_\zeta^2-14S_\zeta\\&-S(S+1)+9]+V_+(S_+^4+S_-^4)+V_-(S_+^4-S_-^4),\end{aligned} \tag{4}$$

where $S_\pm=S_\xi\pm iS_\eta$.

Since we do not observe all possible transitions between the six levels, we are not able to determine the 13 parameters allowed by symmetry. The number of parameters used in the analysis of the data was reduced by reason of the following physical arguments. In cubic symmetry the shift of the g factor from the free-electron value of 2.0023 is usually small. The anisotropy of this shift in C_s symmetry is expected to be less than the shift and, therefore, we neglect it and assume the g tensor to be isotropic. Anisotropic g tensors for S-state ions in low symmetry have been observed by Schneider *et al.*[29] in mixed crystals of ZnS_xSe_{1-x}. Our isotropy approximation is likely to fail in the case of ZnTe, where in cubic symmetry the shift is 5% of the g factor.[30] In terms of the reduced number of parameters, Eqs. (2) and (3) may then be written

$$\mathcal{H}=g_0\beta\mathbf{H}\cdot\mathbf{S}+D[S_z^2-\tfrac{1}{3}S(S+1)]+E(S_x^2-S_y^2), \tag{5}$$

as in Sec. I, Eq. (1). The x, y, and z coordinates do not correspond to the crystal coordinates ξ, η, and ζ but are the directions of the principal axes of the observed g tensor. The fourth-order terms are then used as in Eq. (4) with $\zeta=z$, $S_\pm=S_x\pm iS_y$, and $U_-=V_-=0$. The terms that involve these last two coefficients again are related to the orientation of the quartic terms relative to the crystal coordinates and we make a simple choice. This choice is made so that when $F/V_+=\sqrt{5}/3$ we obtain the usual cubic crystalline field terms aligned along the x, y, and z coordinate system. The number of parameters is then reduced to seven: g, D, E, F, U, V, and τ, the orientation of the x and y coordinates with respect to the crystal coordinates ξ and η.

The spin Hamiltonian with an E and a D term in addition to the Zeeman term has been discussed by several authors[4,5,16] and was reviewed in Sec. I. The experimental g factors, defined as the ratio of βH to the microwave quantum, are calculated for the cases $D\neq0$, $E=0$ and $D=0$, $E\neq0$. The energy levels in zero magnetic field consist of three Kramers doublets. In the first case the lowest doublet has $g_z=2$ and $g_x=g_y=6$ when $D>0$, with g_x and g_y splitting away from 6 when $E/D\ll1$. The other two doublets have two of the g factors very small or zero and no paramagnetic resonance absorption is expected. The second case results in $g_z=0.607$, $g_x=0.857$, and $g_y=9.678$ for the lowest doublet and an isotropic $g=4.29$ for the central doublet. When $D/E\ll1$ this isotropic factor splits into three components, with g_x and g_z moving away from 4.29. The discussion has been extended[5,16] and very useful graphs of the experimental g factors as a function of E/D have been given. The terms S_x^2, S_y^2, and S_z^2 are linearly dependent and a change of coordinates is always possible, which makes $E\leq D$. If, in addition, the order of the levels is not considered important, all the results may be examined for $0\leq|E/D|\leq\frac{1}{3}$. Such graphs are shown in Fig. 11 and include curves when the microwave quantum is comparable to D. Such graphs were used to obtain approximate fits of our data to the spin Hamiltonian.

B. Parameter Determination

Fits of the spin-Hamiltonian parameters to the experimental results have been made. We employed the nonlinear least-squares program of Marquardt,[31] in which the parameters are varied until a least-squares fit to the observations is obtained. In order to take the frequency dependence into account, the observed g factors were computed as the ratio of the eigenvalue differences to βH, and H was varied until this difference equaled the microwave quantum. Any number of the parameters D, E, F, U, V, g_0, and ν could be varied. Usually D was set equal to unity and the results were then obtained in units of D.

In the discussion of the previous section, where the

[27] F. S. Ham and G. W. Ludwig, in *Proceedings of the First International Conference on Paramagnetic Resonance, Jerusalem, 1962*, edited by W. Low (Academic Press Inc., New York, 1963), Vol. 1, p. 130; F. K. Kneubuhl, Phys. Letters **2**, 163 (1962).

[28] F. S. Ham, J. Phys. Chem. Solids **24**, 1165 (1963).

[29] J. Schneider, B. Dischler, and A. Raüber, J. Phys. Chem. Solids (to be published).

[30] J. C. Hensel, Bull. Am. Phys. Soc. **9**, 244 (1964).

[31] D. W. Marquardt, J. Soc. Ind. Appl. Math. **11**, 431 (1963); IBM SHARE Library, Distribution No. 309401, NLIN2 (unpublished).

general form of the spin Hamiltonian is derived, the z axis was taken to be the one perpendicular to the symmetry plane. On the other hand, the experimental results are labeled such that the y axis is perpendicular to the symmetry plane. The particular transformation of axes between these sets of coordinates is $(x'y'z')\rightarrow(zxy)$, where in the primed system the z' axis is perpendicular to the symmetry plane and the unprimed system corresponds to the experimental results, as in Fig. 1 and the Tables. The parameters of the quadratic terms in the spin Hamiltonian, D and E, are readily transformed under the transformation of axes. However, the quartic terms are more cumbersome to transform and the number of parameters in the transformed spin Hamiltonian is larger than the number used in the fitting. Therefore, in the one case where we quote fits employing quartic terms, ZnS:Fe–Cu, we do so in the primed coordinate system with z' perpendicular to the symmetry plane. These results appear only in the bottom of Table II.

For ZnS:Fe–Ag the five g factors in Table IV were used and a three-parameter fit was obtained with $F=U=V$ set equal to zero. The angle τ never enters the calculation and g_z for the lowest doublet was omitted. The results are shown in Table IV and correspond to $E/D=0.0764\pm0.0002$ and $h\nu/D=0.934\pm0.006$. The difference between observed and calculated g factors is less than 0.006. The experimental points have been plotted in Fig. 11 at this value of E/D. No significant improvement could be obtained by adding quartic terms to the spin Hamiltonian.

The results for ZnS:Fe–Cu are not as clear cut. The seven values of g obtained at 9 GHz in Table II were used to obtain fits, and values at 24 GHz were computed and compared. The value of g_y for the lowest Kramers doublet was omitted in the calculations because of its uncertainty. With the quartic terms set equal to zero, a fit is obtained with $E/D=0.373\pm0.004$ and $|h\nu/D|=0.435\pm0.095$. The difference between the observed and the calculated g factors is less than 0.08. The quality of this fit is not nearly as good as the one for ZnS:Fe–Ag. The experimental g factors have been plotted in Fig. 11 at a value of $E/D=0.296$, the value obtained from the fit with the appropriate change in coordinates. The reason for the difficulty in fitting with three parameters is now apparent from examining this figure. The observed g factors for the central doublet are such that the upper and middle ones are closer together than the middle and the lower ones. In the calculated curves, though, just the opposite occurs for all values of E/D. The frequency dependence does not change this feature near $E/D=0.3$. A spin Hamiltonian more complicated than Eq. (1) is therefore needed to fit the ZnS:Fe–Cu results. Fits of somewhat better quality were obtained with the inclusion of one quartic term. The results are shown in Table II. Additional quartic terms did not improve the fits further. The fit is still not as good as

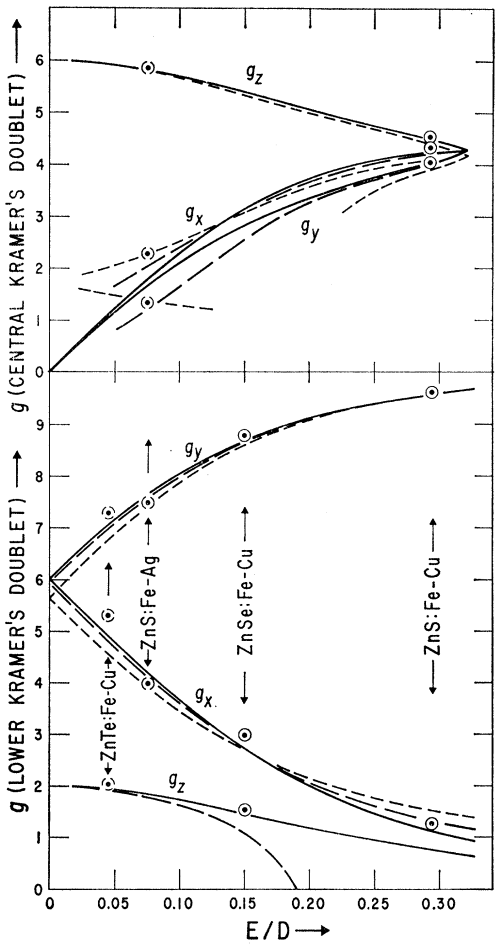

FIG. 11. The theoretically derived observed g-factor dependence of the lower two Kramers doublets on E/D is shown for $h\nu/D$ equal 0.001 by the solid line, 0.5 by the dashed line, and 1 by the short dashed line. The experimental results are plotted as discussed in the text. For ZnS:Fe–Cu the E/D ratio is 0.373. However, the axes have been appropriately relabeled in order that E/D be less than 0.33. In this case it is 0.296.

the ZnS:Fe–Ag case and may be a result of the breakdown of the approximations made in the spin Hamiltonian. A systematic error in the observations may also account for the fitting difficulties, especially errors in g' and g'' (see Table II) which are sensitive to misalignment of the crystals in the magnetic field.

A fit was obtained for the ZnSe:Fe–Cu case with $E/D=0.1386$, $h\nu/D=0.2218$, and $g_0=2.058$, which reproduces the observations.

A fit for ZnTe:Fe–Cu again proved difficult to obtain. Figure 11 indicates that g_0 should be taken larger than 2.0 in order to fit the large g factors. The small g factor is then calculated to be too large and the frequency dependence is such that it cannot improve the fit substantially. We find $E/D=0.040$ and $g_0=2.11$. The data indicate that D is larger here than in all

TABLE V. Symmetry properties of cation associates out to the 15th nearest neighbor.

Neighboring cation shell number	Number of distinct sets of the following symmetry 4 centers of C_{3v}	6 centers of C_{2v}	12 centers of C_s	24 centers of C_1
1			1	
2		1		
3			2	
4			1	
5				1
6	2			
7				2
8		1		
9			3	
10				1
11			2	
12			2	
13				3
14				2
15			1	

other cases, but it is not possible to determine its magnitude from the measurements at 9 GHz.

The zero-field splittings of our most complete examples are shown below.

Associate	Lower to center Kramers doublet (cm^{-1})	Center to upper Kramers doublet (cm^{-1})
ZnO:Fe–Li	0.24	0.48
ZnS:Fe–Ag	0.69	1.29
ZnS:Fe–Cu	2.43	2.66
ZnSe:Fe–Cu	3.23	5.34

C. Model

It has been shown that the paramagnetism arises from the ^6S state of Fe^{3+} perturbed by large electric fields; that a diamagnetic Cu^+ ion is a nearby impurity; and that the Fe^{3+} is at a site having C_s symmetry. It is most likely that both the Fe^{3+} and Cu^+ ions occupy cation sites since this provides local charge compensation. The first 15 neighboring cation-site associates have the symmetry properties shown in Table V. Thus, out to the 15th nearest associate sites, nearest, fourth nearest, and 15th nearest cation sites are the only associate sites having a single pair of twelve equivalent sites of C_s symmetry. While some other associates also result in C_s symmetry, such as third nearest associate sites, these produce a number of somewhat different spectra corresponding to the number of nonequivalent groups of the associate, e.g., for the third nearest associate there are two nonequivalent groups. Since only a single group of spectra was observed, only the first, fourth, or 15th nearest associates are possible. The 15th associate, as well as the fourth, is not a likely possibility in light of the following argument involving the copper hyperfine interaction. Moreover, if the fourth nearest associate were the one observed in our spectra, we would expect to see also other associates. Since only a single C_s symmetry spectrum was observed, it must then result from the nearest associate.

The magnitude of the Fe^{57} hyperfine interaction for ZnS:Fe–Cu is 7.9 G, while that for isolated substitutional Fe^{3+} in ZnS is 1.5 G and in ZnSe is 1.3 G.[32] The hyperfine interaction with Cu^{63} for the Fe–Cu associate in ZnS is 3.4 G. If this is scaled by the gyromagnetic ratio, as found by Estle and Holton[32] to be the empirical rule for the superhyperfine structure of isolated $3d$ impurities in II–VI compounds, the equivalent interaction with Zn^{67} is 0.82 G. This is consistent with the limits on the nearest Zn^{67} ion hyperfine interaction found for isolated Fe^{3+} (<2.6 G in ZnSe and $\lesssim 3.2$ G in ZnTe) and comparable to the values observed for Mn^{2+} and Cr^+.[32] These results are consistent with the Fe^{3+} and Cu^+ ions occupying nearest substitutional zinc sites. Association involving one or more interstitials is generally in poor agreement with the results.

Thus, the paramagnetism arises from the ^6S state of Fe^{3+} perturbed by large electric fields at the Fe site which are due to the charged Cu^+ associate at the nearest substitutional Zn site and a crystalline distortion near the iron site. The model is shown in Fig. 1. The impurities charge-compensate one another so that the resulting associate is neutral in the lattice. Both impurities have relatively stable electron configurations.

For an S-state ion there may not be a linear relationship between the spin-Hamiltonian parameters and the electric field gradients. Nevertheless, a spin Hamiltonian consistent with this model can be made up from axially symmetric fields which lie in the symmetry plane. The Fe–Cu in the ZnTe case experiences a dominant axial field directed nearly along a $\langle 111 \rangle$ crystal axis. The spin Hamiltonian may be simply written as DS_z^2. The Fe–Cu in the ZnS cases is nearly pure "rhombic," requiring the spin-Hamiltonian term $E(S_x^2-S_y^2)$. The origin of the S_y^2 term, which would seem to require an electric field perpendicular to the symmetry plane, may be seen by first writing the term as $\alpha S_z^2+\beta S_x^2$. The axial fields are in the z and x directions in the symmetry plane and may arise from the charge on the copper ion, a slightly different charge on the in-plane sulfur ion, or displacements of these ions and the Fe^{3+} from exact lattice sites in the x-z plane. In order to achieve the desired form, let $\beta=2\alpha$ and subtract $\alpha S^2=\alpha(S_x^2+S_y^2+S_z^2)$, which only changes the zero of energy. The remaining cases are intermediate between these two.

[32] T. L. Estle and W. C. Holton, Phys. Rev. **150**, 159 (1966); throughout this section the convention $|D| \geq 3|E|$ will be employed.

Each of the cases investigated in detail is shown in Fig. 11. Here the theoretical prediction of the observed g factors, neglecting fourth-order terms in the spin Hamiltonian, are plotted as a function of E/D. This is done for various ratios of $h\nu$ to D and $g_0=2$. Overlaid on this figure are the observed g factors for each of the cases studied. The value of E/D assigned to each case is that value obtained from fitting the spin-Hamiltonian parameters. It is seen that no special relationship exists to produce a pure "rhombic" field at the Fe site; and, in fact, all ratios of E/D seem to occur.

It is known that it is always possible to relabel axes and keep the ratio $|E/D| \leq \frac{1}{3}$. A discussion of this point has been given in Refs. 5 and 16. In Fig. 11, only the g-factor dependence on E/D for the two lower Kramers doublets and for $E/D \leq \frac{1}{3}$ is shown. The axes as shown for the model (see Fig. 1) are consistent with $E/D \leq \frac{1}{3}$ in Fig. 11, with the exception of ZnS:Fe–Cu. The g factors related to the upper Kramers doublet are not shown in Fig. 11, since these resonances were never observed. The absence of these resonances is not entirely unexpected because these levels are less populated in our case at 1.3°K and because the g factors and transition probabilities are less favorable for the upper Kramers doublet than for the central Kramers doublet. Curves are also shown in Fig. 11 for $h\nu$ comparable to D. In this case the energy-level separation does not always increase with increasing magnetic field strength and sometimes more than one transition between a pair of levels is possible or no transition is possible until the field becomes quite large. In fact, the system cannot usually be described by effective g values. This accounts for these plots being incomplete.

Although it is possible to always have $|E| < |D|$, for theoretical considerations it is useful to consider the case $E \neq 0$, $D=0$, and how it can be obtained from the ligand crystal fields. Griffith[19] has shown that in low symmetry the D and E terms in the spin Hamiltonian may arise from the spin-orbit interaction, as $-\lambda^2 \Lambda_{ij} S_i S_j$, where

$$\Lambda_{ij}=\sum_{n\neq 0} \langle 0 | L_i | n \rangle \langle n | L_j | 0 \rangle / (E_n - E_0), \quad (6)$$

with primarily one excited state n contributing. In pure T_d symmetry the spin-orbit interaction connects the $^6A_1$ ground state only with $^4T_1$ terms. The relative sizes of the D and E terms are then related to the splitting of this $^4T_1$ level in the low symmetry. In particular, when the T_1 state is split into three equally spaced components, one obtains $E \gg D$, provided all other contributions to D and E are much smaller than E. We wish to consider a four-coordinated compound MA^2BC as an approximate description of the Fe–Cu associates. Here M represents the Fe ion, A the sulfur ions which lie outside the symmetry plane, and B and C the sulfur ions which lie in the symmetry plane. Ion B is adjacent to the Cu ion and ion C is considered to differ from ions A. We consider the complex oriented with the B and C ions in the $(1\bar{1}0)$ plane with the z axis bisecting the MB, MC directions. The A ions are in the (110) plane. In addition to the fields from the neighboring sulfur ions the complex may be distorted and we assume this to be along the [001] or z direction. The Cu^+ ion also generates a field at the iron site M. The crystalline field may then be approximated by[19]

$$\begin{aligned} V_c = {} & 2AV(A_1, i) + CV(A_1, i) + BV(A_1, i) \\ & - 2AV(T_2, z) - BV(T_2, z) + (\sqrt{6})BV(T_2, \rho) \\ & + (\sqrt{3})CV(T_2, \tau) + JV(T_2, z) \\ & + IV(T_2, x) + IV(T_2, y), \quad (7) \end{aligned}$$

where A, B, C are now the strengths of the fields from the respective ligands, J the strength due to the distortion and $\sqrt{2}I$ that due to the Cu ion, and $V(a, \alpha)$ is an irreducible tensor operator belonging to the component α of the irreducible representation a of the group T_d.[19] The trigonal component ρ transforms as the linear combination $(-f_x - f_y + 2f_z)/\sqrt{6}$ of the x, y, and z components of $V(T_2)$ and τ as $(f_x + f_y + f_z)/\sqrt{3}$. Of the terms in the potential only those transforming as T_2 split the $^4T_1$ terms. In particular, the $V(T_2, z)$ components split this term into three equally spaced levels, but $V(T_2, \rho)$ and $V(T_2, \tau)$ do not. If now the coordinates are transformed so that the z and x axes lie in the symmetry plane BMC, the spin Hamiltonian takes the form of Eq. (1). The case $E \neq 0$, $D \cong 0$ obtains only when the terms of symmetry $V(T_2, x)$ and $V(T_2, y)$ in Eq. (7) vanish. This condition requires $C - B + I = 0$, which is a special relationship among the various field strengths and is not related to symmetry. Again, these considerations indicate that the occurrence of the case $E \neq 0$, $D \cong 0$ is accidental, as is borne out by the observation of a variety of $|E/D|$ ratios in the chalcogenides.

At this point it should be emphasized again that in the above arguments an ionic description is employed. It is known that the observed positive g shifts in the chalcogenides cannot be explained with such a model and, therefore, there are other excited states, such as those involving a charge transfer to and from the ligands, which have to be taken into account.[22]

V. DISCUSSION

A defect consisting of an Fe^{3+} ion associated with a monovalent impurity at a nearest cation site explains the results of our EPR measurements on a large number of II–VI compounds. In some instances the experimental evidence together with physical plausibility leads directly to this model. In other cases the evidence is less convincing, but this is still the simplest explanation in general. When Fe^{3+} associates with monovalent impurities at nearest cation sites in II–VI semiconducting compounds, the quadratic spin-Hamiltonian param-

eters are large but a variety of values of $|E/D|$ occur, including values near $\frac{1}{3}$. However, no special preference is shown for $|E/D|$ near $\frac{1}{3}$, the value which leads to the excited Kramers-doublet g value of 4.3. This conclusion regarding Fe^{3+} in II–VI compounds is reinforced by the recent observations of Morigaki and Hoshina[33] on Fe^{3+} associates in CdSe. They observe a large D and $|E/D|$ sufficiently close to $\frac{1}{3}$, so that somewhat anisotropic lines near $g=4.3$ are observed. They, apparently, see only one of the three possible types of associates rather than all three, as we saw for ZnO:Fe–Li. Another difference from our results is the photosensitivity of the spectrum. None of the centers studied in this paper are photosensitive.

Observations of Fe^{3+} in noncubic sites of other crystals lead to conclusions similar to those for the II–VI compounds. Of approximately 15 other cases,[5–13,15] in which iron has been observed to have $|D|\geq 0.3$ cm^{-1} in single crystals, four of these have $|E/D|\geq 0.22$ and thus yield lines near $g=4.3$. Some of the 15 have $E=0$ because of axial symmetry. The four cases consist of $MgWO_4$ studied by Peter,[11] $ZnWO_4$ studied by Nilsen and Kurtz,[12] topaz studied by Denison *et al.*,[7] and $CaWO_4$ studied by Kedzie *et al.*[13,34] and Kirton and Newman.[35] In the first three cases, the iron occupies the low-symmetry substitutional site in the crystal. However, Kedzie *et al.*[13] attribute their results to a slight distortion of the S_4 symmetry of a tungsten site. This explanation suffers from a number of serious difficulties, which include the abnormally large value of the quartic cubic-field parameter required in the nearly tetrahedral oxygen environment (it must be roughly 1 cm^{-1}); the inconsistency of the charge imbalance of three units and the small perturbation of the charge compensating impurity, which must be the agent for the slight distortion; and the difficulty of getting the observed g tensor from the model suggested. A physically plausible and perfectly satisfactory explanation of the results is that the Fe^{3+} is in a large noncubic crystalline field of C_1 symmetry arising from association (such as Na at a Ca site and Fe at an adjacent Ca site) together with the S_4 symmetry of the cation site. Quadratic terms in the spin Hamiltonian would be of primary importance. It should be pointed out that such a model would require a reinterpretation of Kedzie's experimental results. The spectra observed by Kedzie *et al.*[13,34] would arise from an excited state. This has, in fact, been suggested by Kirton and Newman.[35] This would then mean that all published cases for lines near $g=4.3$ arising from Fe^{3+} in single crystals result from fortuitous values of E and D for the low-symmetry sites. There is one exception to this generalization and it is FeS_2Se_2 centers in mixed $ZnS_{1-x}Se_x$ crystals.[29] In this case $|E/D|=0.29$.

Although it is possible to have $|E/D|$ nearly $\frac{1}{3}$ for special intermediate symmetries, as suggested by Castner *et al.*[4] and explored in depth by Griffith,[19] we see that the majority of the cases studied for single crystals, where $|E/D|$ is near $\frac{1}{3}$, do not correspond to cases of intermediate symmetry. In fact, the idea that $|E/D|$ is near $\frac{1}{3}$ for certain special arrangements of ligands is likely to hold only for special cases in which the nuclear displacements accompanying the substitution of different ligands do not produce effects as big as those resulting from the changes in the ligand bond strengths.

There still remains the question of the origin of the lines near $g=4.3$ in glasses.[4] Castner *et al.*[4] attribute this to special ligand arrangements in these amorphous materials. We would suggest that the evidence of the single-crystal results can be extrapolated to this case and leads to a more plausible explanation. Instead of rather unique environments, we would postulate that the Fe^{3+} resides in a variety of environments of low symmetry, including values leading to lines near $g=4.3$. Since the environments which do not produce the lines near $g=4.3$ will produce spectra with extremely large anisotropies in general, they will in the amorphous material average out to give a broad weak background. The $g=4.3$ lines will, however, lead to a sharp peak in the absorption. Thus, the lines at a g value of 4.3 in amorphous materials are quite likely simply a consequence of the fact that the only isotropic effective g value allowed for $S=\frac{5}{2}$ resulting from a large noncubic quadratic fine-structure Hamiltonian is 4.3, and this value is selectively peaked by the variable environments.

ACKNOWLEDGMENTS

We would like to acknowledge the many interesting discussions with our colleagues both in Dallas and Freiburg and, especially, to thank Professor C. P. Slichter and Dr. A. Räuber for their interest and stimulating comments during the course of this work. We would like to thank Dr. G. D. Watkins for taking a powder EPR pattern at 19 GHz. We also thank R. D. Stinedurf and F. Friedrich for assistance in the preparation of crystals. Thanks are due to D. Powell for programming a number of the calculations.

[33] K. Morigaki and T. Hoshina, J. Phys. Soc. Japan **23**, 318 (1967).
[34] R. W. Kedzie and D. H. Lyons, Phys. Rev. Letters **15**, 632 (1965).
[35] J. Kirton and R. C. Newman, Phys. Rev. Letters **15**, 244 (1965).